Supporting Information for "Anthropogenic contributions to the 2021 Pacific Northwest heatwave"

Emily Bercos-Hickey[1], Travis A. O'Brien[2,1], Michael F. Wehner[1], Likun Zhang[3,1], Christina M. Patricola[4,1], Huanping Huang[1], Mark D. Risser[1]

[1]Climate and Ecosystem Sciences Division, Lawrence Berkeley National Laboratory, Berkeley, California, USA

[2]Department of Earth and Atmospheric Sciences, Indiana University, Bloomington, Indiana, USA

[3]Department of Statistics, University of Missouri, Columbia, Missouri, USA

[4]Department of Geological and Atmospheric Sciences, Iowa State University, Ames, Iowa, USA

1. Non-stationary GEV analysis

The non-stationary generalized extreme value (GEV) analysis on individual station data uses a GEV distribution with a location parameter linearly dependent on a sum-total forcing variable for five well-mixed greenhouse gases (WMGHGs) to accommodate non-stationarity (Risser et al., 2021). The five WMGHGs include carbon dioxide, CFC-11 and CFC-12 halocarbons, methane and nitrous oxide, whose concentration values come from Meinshausen and Vogel (2016) and Meinshausen and Nicholls (2018) and whose forcing formulae can be found in Etminan, Myhre, Highwood, and Shine (2016) and Hodnebrog et al. (2013). To estimate the GEV parameters, we impose a non-informative

prior on the shape parameter (Zhang & Shaby, 2022), and then run a Metropolis-Hastings algorithm to draw samples from the posterior distributions of the parameters. Since the GEV distribution has a finite upper bound when the shape parameter is negative, we can directly examine the posterior distribution of the upper bound.

2. Configuration of the Weather Research and Forecast (WRF) model

Some simulations of the PNW heatwave in this study were performed using the Weather Research and Forecasting (WRF) model (Skamarock et al., 2008) version 3.8.1. Model output was generated every hour with 50 vertical levels from a grid with horizontal spacings of either 18 km or 50 km. The WRF simulation domains are shown in Figure S2a. Parameterization schemes used in all simulations include: the Rapid Radiative Transfer Model for Global Climate Models (Iacono et al., 2008) short and longwave schemes, the WRF single-moment 6-class microphysics scheme (Hong & Lim, 2006), the Noah land surface model scheme (Chen & Dudhia, 2001), the Medium Range Forecast (MRF) boundary layer scheme (Hong & Pan, 1996), and the Grell-Freitas ensemble cumulus scheme (Grell & Freitas, 2014). Ten-member ensembles at both grid spacings were generated using the Stochastic Kinetic Energy Backscatter Scheme (SKEBS) (Shutts, 2005; Berner et al., 2011). SKEBS uses random stream function perturbations to represent model uncertainty from unresolved scales and has previously been used to generate WRF ensembles (Berner et al., 2011; Patricola & Wehner, 2018). The daily maximum temperature and geopotential height contours at 500 hPa on June 28, 2021 are shown for the ten ensemble members at 18 km and the ensemble average in Figure S3.

3. Configuration of the International Centre for Theoretical Physics Regional Climate Model (RegCM)

Some simulations of the PNW heatwave in this study were performed using the International Centre for Theoretical Physics RegCM4 regional model (Giorgi et al., 2012). The simulations were configured with 18 km and 50 km horizontal grid spacings and 30 sigma levels with a model top pressure of 50 hPa, a timestep of 36 seconds, and model output saved every 3 hours. The RegCM simulation domains are shown in Fig. S2b. The simulations used hydrostatic dynamics, the National Center for Atmospheric Research (NCAR) Community Climate Model 3 radiation parameterization (Kiehl et al., 1996), the University of Washington turbulence closure and planetary boundary layer parameterization (Grenier & Bretherton, 2001; O'Brien et al., 2012), the Massachusets Institute of Technology convection parameterization (Emanuel, 1991; Emanuel & Živković-Rothman, 1999), and the Biosphere Atmosphere Transfer Scheme 1e (Dickinson et al., 1993). Ensemble simulations at 18 km and 50 km resolution were generated by pertrubing the intitial and boundary condition temperature field by 0.1% (O'Brien et al., 2011). The daily maximum temperature and geopotential height contours at 500 hPa on June 28, 2021 are shown for the ten ensemble members at 18 km and the ensemble average in Figure S4.

The RegCM 4.9.5 simulations are based on the master branch of the github code at commit `8197f9`, with an additional bug fix applied that allows the code to run at the National Energy Research Supercomputing Center (NERSC). (This bug fix was merged with the master branch of the code in commit `6b43573`.)

4. Model Validation

To establish the validity of the heatwave simulations, we compare the WRF and RegCM hindcasts, the datasets that provided their initial and boundary conditions (ICBCs), NARR and GFS, respectively, and the GHCN observational data. Figure 3a shows the June 25-July 1, 2021 daily maximum temperature averaged over the region 45°N-52°N and 124°W-119°W (Figure S2) from the GHCN (black), ensemble-averaged WRF historical simulations (blue, solid), NARR (blue, dashed), ensemble-averaged RegCM historical simulations (red, solid), and GFS (red, dashed). The shading around the WRF and RegCM lines show the range of values from the 10-member ensembles. From Figure 3a, the NARR and GFS are over 6°C cooler than the GHCN and about a day late in reaching the hottest temperatures. The timing and magnitude of the daily maximum temperatures throughout the heatwave from the WRF and RegCM models are mostly in close alignment with the NARR and GFS, respectively. The differences between the WRF and the NARR and the RegCM and the GFS seen in Figure 3a are not surprising and are likely due to the models departing from their initial conditions and the chosen parameterization schemes. Although both models and the data used for their ICBCs produce a cooler and delayed heatwave, WRF and RegCM are consistent with each other in their simulations of the heatwave event despite using different ICBCs and parameterizations.

To further examine the validity of the WRF and RegCM hindcasts, we compare the models with the European Centre for Medium-range Weather Forecasts (ECMWF) reanalysis five (ERA5) (Hersbach et al., 2020) on June 28, 2021, the hottest day of the heatwave from the GHCN (Figure 3a). Figure S5 shows the daily maximum temperature and 500 hPa height contours from (a) the ERA5, (b) the ensemble-averaged WRF his-

torical simulations, and (c) the ensemble-averaged RegCM historical simulations. Figure S5a shows the high temperatures and omega blocking pattern that were distinct features of the PNW heatwave. Figures S5b,c show that the WRF and RegCM models are correctly replicating the key features of the heatwave, thus lending confidence to the hindcast simulations.

Lastly, we examine how the horizontal spatial resolution may affect the hindcast simulations. The effects of resolution on the WRF and RegCM simulations can be seen in Fig. S6, which shows the June 25-July 1, 2021 time series of the spatially averaged (see Figure S2) daily maximum temperature from the GHCN, NARR, GFS, and the ensemble averages of the 18 km and 50 km WRF and RegCM historical simulations. For the WRF model, Figure S6 shows that there is little difference between the daily maximum temperature at 18 km and 50 km. For the RegCM model, Figure S6 indicates that the daily maximum temperature is similar between the two resolutions, with a notable exception on June 29 where it is cooler at 18 km than at 50 km.

Figures S7 and S8 show the daily maximum temperature and geopotential height contours at 500 hPa on June 28, the hottest day of the heatwave according to the GHCN (Figure S6), for the ten ensemble members and the ensemble average from the 50 km historical simulations of the WRF and RegCM models, respectively. A comparison of Figures S3 and S7 reveals that the WRF model simulates the omega blocking pattern and high temperatures of the heatwave at both resolutions. Similarly, a comparison of Figures S4 and S8 indicates the the RegCM model also simulates the omega blocking pattern and high temperatures at both resolutions.

To visualize the differences between the 18 km and 50 km resolution simulations, Figure S9 shows the ensemble average of the daily maximum temperature on June 28 from the (a) 18 km WRF, (b) 50 km WRF, (d) 18 km RegCM, and (e) 50 km RegCM historical simulations. The difference between the daily maximum temperature in the 18 km and 50 km ensemble averages is shown for the (c) WRF and (f) RegCM models. From Figure S9a,b, the WRF model is capturing the high temperatures associated with the heatwave event at both resolutions. Figure S9c indicates that, for most of the region affected by the heatwave, the 18 km simulations are 0-2°C warmer than the 50 km simulations. From Figure S9d,e, the RegCM model is mostly capturing the high temperatures associated with the heatwave, although temperatures in eastern Washington are notably lower in the 50 km simulations. In contrast to the WRF model, the difference between the RegCM 18 km and 50 km simulations (Figure S9f) shows large positive and negative anomalies throughout the domain. The anomalies in Figure S9f are likely due to the elevation differences between the two resolutions, where the 50 km simulations will not resolve terrain as well as the 18 km simulations. The 50 km simulations are therefore warmer in higher elevation regions such as the North Cascades and the Sierra Nevada Mountains. Although the choice of resolution does not strongly affect the ability of the WRF and RegCM models to capture the overall characteristics of the PNW heatwave (see Figures S3, S7, S4, and S8), due to the elevation bias present in the 50 km simulations, we use the 18 km WRF and RegCM simulations for the remainder of the analysis.

5. Pseudo-global warming (PGW) / Hindcast Attribution methodology

The PGW Hindcast Attribution method assumes that similar synoptic conditions, mainly the omega block and atmospheric river, that produced the PNW heatwave in the historical time period could happen in past and future climates. This is a restrictive assumption, precluding any statement about how the frequency of such large scale conditions will change. The variables adjusted in the WRF initial and boundary conditions include temperature, relative humidity, geopotential height, sea-level and surface pressure, sea-surface temperature, and surface temperature; for RegCM, only the temperature and specific humidity fields were altered. Additionally, we modified the WRF radiation code to account for different greenhouse gas concentrations of CO_2, CH_4, N_2O, CFC-11, CFC-12 and CCl_4 in the counterfactual climate simulations consistent with pre-industrial and Shared Socioeconomic Pathway 585 (SSP585) (O'Neill et al., 2016) specifications (Meinshausen & Vogel, 2016). Greenhouse gas concentrations were modified in RegCM using built in tables for the year 1850 and for the year 2090 under the SSP585.

The PGW deltas were calculated from the Coupled Model Intercomparison Project Phase 6 (CMIP6) (Danabasoglu, 2019) data by computing a multi-model average (Table S1) and subtracting the 1995-2014 averaged historical simulations from: 1) The averaged hist-nat simulations; 2) The 2040-2060 averaged SSP585 simulations (mid-century); and 3) The 2080-2100 averaged SSP585 simulations (late-century). The length of the historical timeframe was chosen to capture the historical climate and to smooth out any multi-decadal variability. The hist-nat simulation resembles the historical simulation but only includes solar and volcanic forcing (Eyring et al., 2016) and the SSP585 simulation incorporates future emissions and land use changes (O'Neill et al., 2016). Deltas were

calculated for the month of the heatwave event and were added to the corresponding initial and boundary conditions. Hist-nat, mid-century, and late-century simulations were performed with the WRF model, and only nat-hist and late-century simulations were performed with the RegCM model.

References

Berner, J., Ha, S.-Y., Hacker, J. P., Fournier, A., & Snyder, C. (2011). Model uncertainty in a mesoscale ensemble prediction system: Stochastic versus multiphysics representations. *Monthly Weather Review*, *139*(6), 1972-1995.

Chen, F., & Dudhia, J. (2001). Coupling an advanced land surface–hydrology model with the penn state–ncar mm5 modeling system. part i: Model implementation and sensitivity. *Monthly Weather Review*, *129*(4), 569-585.

Danabasoglu, G. (2019). *NCAR CESM2 model output prepared for CMIP6 CMIP.* Earth System Grid Federation. Retrieved from `https://doi.org/10.22033/ESGF/CMIP6.2185` doi: 10.22033/ESGF/CMIP6.2185

Dickinson, R. E., Henderson-Sellers, A., Kennedy, P. J., & Wilson, M. F. (1993). Biosphere atmosphere transfer scheme (BATS) version 1e as coupled for Community Climate Model. *NCAR Tech. Note NCAR/TN-378+SR*(August), 77. doi: 10.1029/2009JD012049

Emanuel, K. A. (1991, nov). A Scheme for Representing Cumulus Convection in Large-Scale Models. *Journal of the Atmospheric Sciences*, *48*(21), 2313–2329. Retrieved from `http://journals.ametsoc.org/doi/10.1175/1520-0469(1991)048%3C2313:ASFRCC%3E2.0.CO;2` doi: 10.1175/1520-0469(1991)048⟨2313:ASFRCC⟩2.0

.CO;2

Emanuel, K. A., & Živković-Rothman, M. (1999, jun). Development and Evaluation of a Convection Scheme for Use in Climate Models. *Journal of the Atmospheric Sciences*, *56*(11), 1766–1782. Retrieved from http://journals.ametsoc.org/doi/10.1175/1520-0469(1999)056%3C1766:DAEOAC%3E2.0.CO;2 doi: 10.1175/1520-0469(1999)056⟨1766:DAEOAC⟩2.0.CO;2

Etminan, M., Myhre, G., Highwood, E., & Shine, K. (2016). Radiative forcing of carbon dioxide, methane, and nitrous oxide: A significant revision of the methane radiative forcing. *Geophysical Research Letters*, *43*(24), 12–614.

Eyring, V., Bony, S., Meehl, G. A., Senior, C. A., Stevens, B., Stouffer, R. J., & Taylor, K. E. (2016). Overview of the coupled model intercomparison project phase 6 (cmip6) experimental design and organization. *Geosci. Model Dev.*, *9*(5), 1937-1958. doi: 10.5194/gmd-9-1937-2016

Giorgi, F., Coppola, E., Solmon, F., Mariotti, L., Sylla, M., Bi, X., ... Brankovic, C. (2012). RegCM4: model description and preliminary tests over multiple CORDEX domains. *Climate Research*, *52*, 7–29. Retrieved from http://www.int-res.com/abstracts/cr/v52/p7-29/ doi: 10.3354/cr01018

Grell, G. A., & Freitas, S. R. (2014). A scale and aerosol aware stochastic convective parameterization for weather and air quality modeling. *Atmos. Chem. Phys.*, *14*(10), 5233-5250.

Grenier, H., & Bretherton, C. S. (2001). A Moist PBL Parameterization for Large-Scale Models and Its Application to Subtropical Cloud-Topped Marine Boundary Layers.

Monthly Weather Review, *129*(3), 357–377. Retrieved from http://dx.doi.org/10.1175/1520-0493(2001)129%3C0357:AMPPFL%3E2.0.CO%5Cn2 doi: 10.1175/1520-0493(2001)129⟨0357:AMPPFL⟩2.0.CO;2

Hersbach, H., Bell, B., Berrisford, P., Hirahara, S., Horányi, A., Muñoz-Sabater, J., ... others (2020). The era5 global reanalysis. *Quarterly Journal of the Royal Meteorological Society*, *146*(730), 1999–2049.

Hodnebrog, Ø., Etminan, M., Fuglestvedt, J., Marston, G., Myhre, G., Nielsen, C., ... Wallington, T. (2013). Global warming potentials and radiative efficiencies of halocarbons and related compounds: A comprehensive review. *Reviews of Geophysics*, *51*(2), 300–378.

Hong, S.-Y., & Lim, J.-O. J. (2006). The wrf single-moment 6-class microphysics scheme (wsm6). *Journal of the Korean Meteorological Society*, *42*(2), 129-151.

Hong, S.-Y., & Pan, H.-L. (1996). Nonlocal boundary layer vertical diffusion in a medium-range forecast model. *Monthly Weather Review*, *124*(10), 2322-2339.

Iacono, M. J., Delamere, J. S., Mlawer, E. J., Shephard, M. W., Clough, S. A., & Collins, W. D. (2008). Radiative forcing by long-lived greenhouse gases: Calculations with the aer radiative transfer models. *Journal of Geophysical Research*, *113*(D13), D13103.

Kiehl, J., Hack, J., Bonan, G., Boville, B., Briegleb, B., Williamson, D., & Rasch, P. (1996). *Description of the NCAR Community Climate Model (CCM3)* (Tech. Rep. No. September). doi: 10.5065/D6FF3Q99

Meinshausen, M., & Nicholls, Z. R. J. (2018). *Uom-remind-magpie-ssp585-1-2-0: Remind-magpie-ssp585 ghg concentrations.* Earth System Grid Federation. Retrieved

from https://doi.org/10.22033/ESGF/input4MIPs.2349 doi: 10.22033/ESGF/input4MIPs.2349

Meinshausen, M., & Vogel, E. (2016). input4mips.uom.ghgconcentrations.cmip.uom-cmip-1-2-0. *Earth System Grid Federation*. doi: 10.22033/ESGF/input4MIPs.1118

O'Brien, T. A., Chuang, P. Y., Sloan, L. C., Faloona, I. C., & Rossiter, D. L. (2012). Coupling a new turbulence parametrization to RegCM adds realistic stratocumulus clouds. *Geoscientific Model Development*, *5*(4), 989–1008. doi: 10.5194/gmd-5-989-2012

O'Brien, T. A., Sloan, L. C., & Snyder, M. A. (2011, sep). Can ensembles of regional climate model simulations improve results from sensitivity studies? *Climate Dynamics*, *37*(5-6), 1111–1118. Retrieved from http://link.springer.com/10.1007/s00382-010-0900-5 doi: 10.1007/s00382-010-0900-5

O'Neill, B. C., Tebaldi, C., Van Vuuren, D. P., Eyring, V., Friedlingstein, P., Hurtt, G., ... Sanderson, B. M. (2016). The Scenario Model Intercomparison Project (ScenarioMIP) for CMIP6. *Geoscientific Model Development*, *9*(9), 3461–3482. doi: 10.5194/gmd-9-3461-2016

Patricola, C. M., & Wehner, M. F. (2018). Anthropogenic influences on major tropical cyclone events. *Nature*, *563*(7731), 339-346.

Risser, M., Wehner, M., O'Brien, J., Patricola, C., O'Brien, T., Collins, W., ... Huang, H. (2021). Quantifying the influence of natural climate variability on in situ measurements of seasonal total and extreme daily precipitation. *Climate Dynamics*. doi: 10.1007/s00382-021-05638-7

Shutts, G. (2005). A kinetic energy backscatter algorithm for use in ensemble prediction systems. *Quarterly Journal of the Royal Meteorological Society*, *131*(612), 3079-3102.

Skamarock, W. C., Klemp, J. B., Dudhia, J., Gill, D. O., Barker, D. M., Duda, M. G., ... Powers, J. G. (2008). A description of the advanced research wrf version 3. *NCAR Technical Note NCAR/TN-475+STR.*.

Zhang, L., & Shaby, B. A. (2022). Reference priors for the generalized extreme value distribution. *Statistica Sinica*. doi: https://doi.org/10.5705/ss.202021.0258

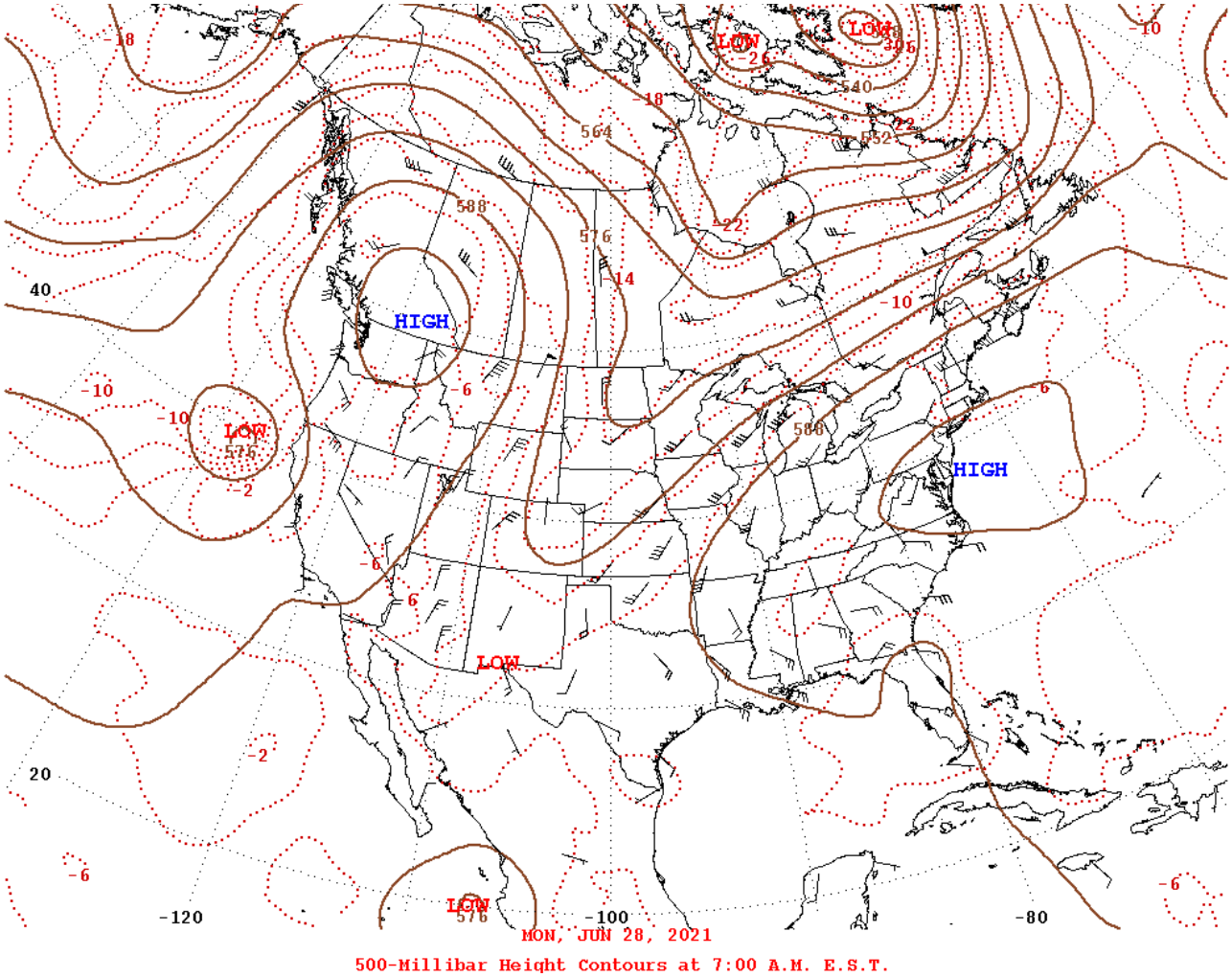

Figure S1. National Oceanic and Atmospheric Administration (NOAA) National Centers for Environmental Prediction (NCEP) 500 hPa height contours on June 28, 2021.

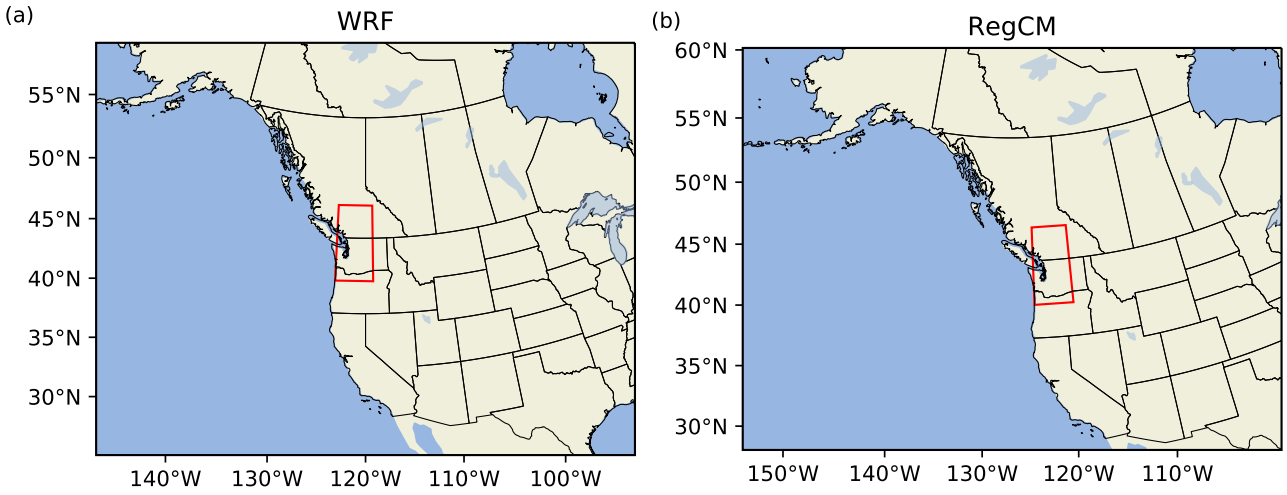

Figure S2. Simulation domains for the (a) WRF model, and (b) RegCM. The red boxes show the region 45°N-52°N and 124°W-119°W, which is used for spatial averaging and is common to both models.

Table S1. CMIP6 models used to calculated the multi-model averaged deltas used in the pseudo-global warming method.

Model
ACCESS-CM2
ACCESS-ESM1-5
CESM2
CNRM-CM6-1
CanESM5
FGOALS-g3
GFDL-CM4
GFDL-ESM4
GISS-E2-1-G
HadGEM3-GC31-LL
IPSL-CM6A-LR
MIROC6
MRI-ESM2-0
NorESM2-LM

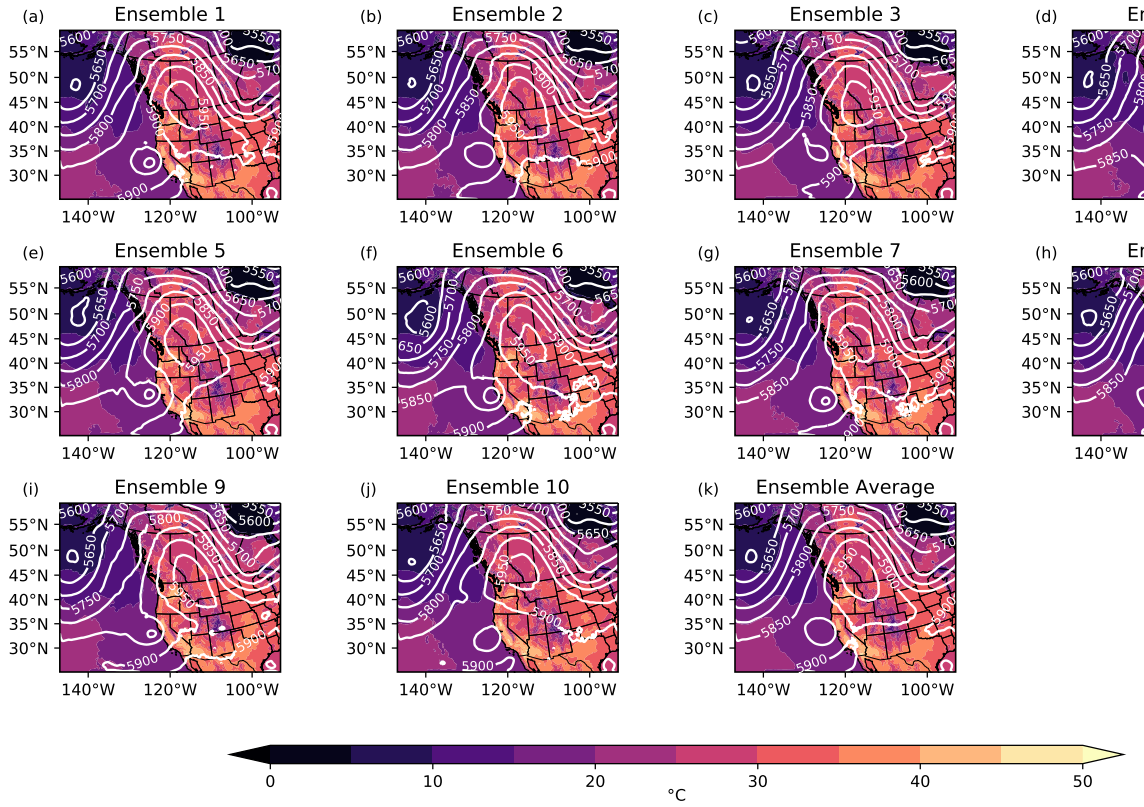

Figure S3. Historical 18 km WRF simulation (a)-(j) individual ensemble members and (k) ensemble-average of the daily maximum 2 m temperature (°C; color contours) and geopotential height at 500 hPa and 0000 UTC (m; white contour lines) on June 28, 2021.

Table S2. Summary of model experiments, where an X indicates that an experiment was performed for the given model.

Experiments	WRF 18km	WRF 50km	RegCM 18km	RegCM 50km
Historical	X	X	X	X
Hist-nat	X	X	X	X
Mid-century	X	X		
Late-century	X	X	X	X
Hist-nat with soil moisture delta	X			
Mid-century with soil moisture delta	X			
Late-century with soilt moisture delta	X			

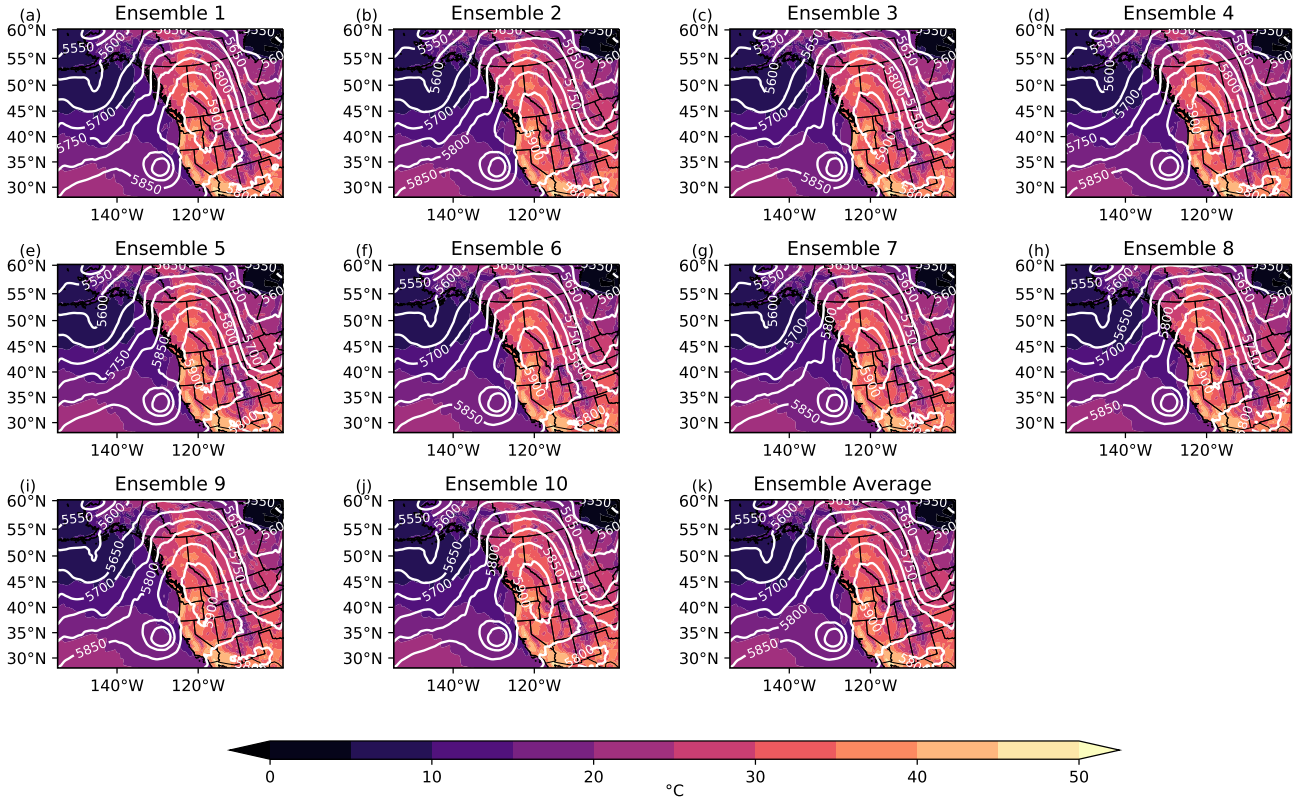

Figure S4. Historical 18 km RegCM simulation (a)-(j) individual ensemble members and (k) ensemble-average of the daily maximum 2 m temperature (°C; color contours) and geopotential height at 500 hPa and 0000 UTC (m; white contour lines) on June 28, 2021.

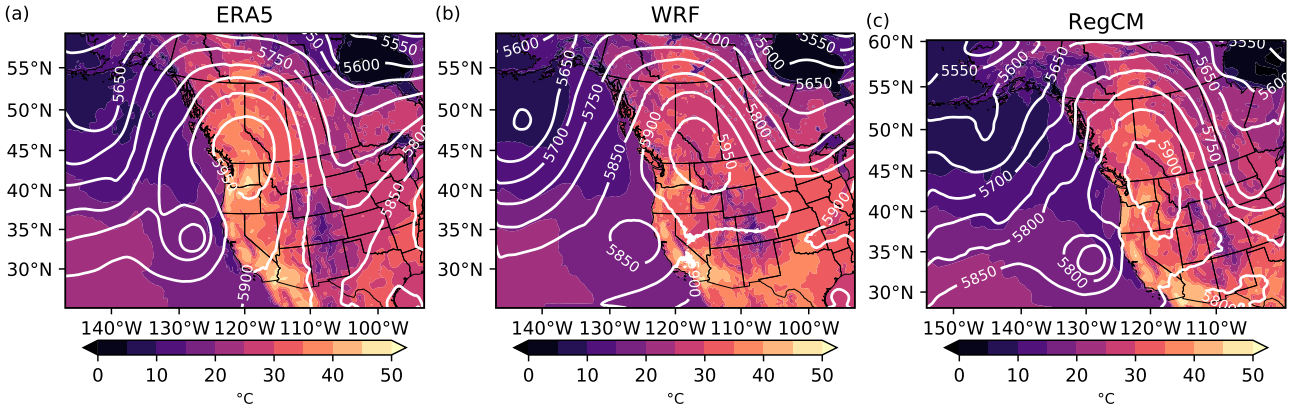

Figure S5. June 28, 2021 (a) ERA5, (b) WRF 18 km historical ensemble average, and (c) RegCM 18 km historical ensemble average of the daily maximum 2 m temperature (°C; color contours) and geopotential height at 500 hPa and 0000 UTC (m; white contour lines).

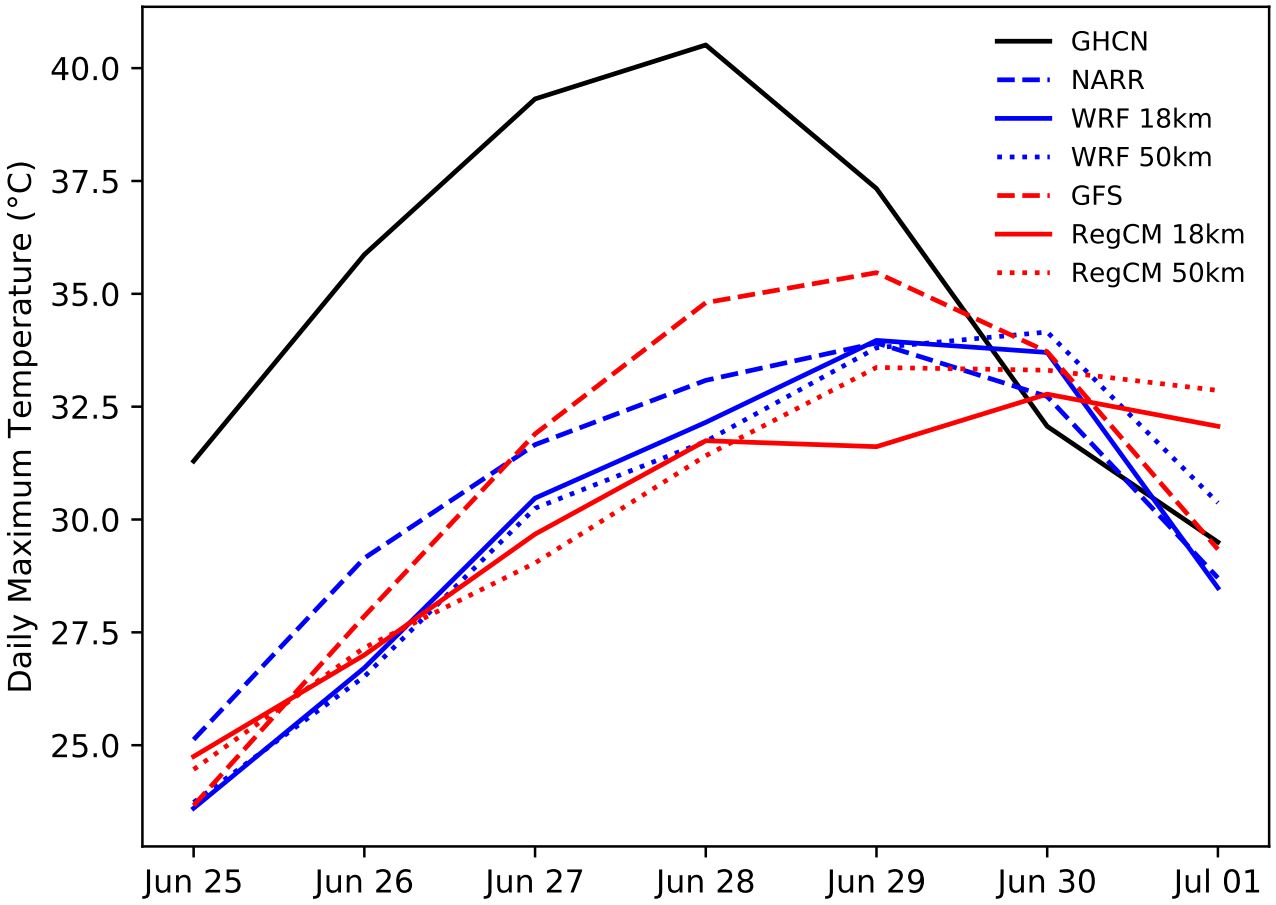

Figure S6. Time series from June 25-July 1, 2021 of the spatially averaged daily maximum temperature from the GHCN (black), NARR (blue, dashed), GFS (red, dashed), the 18 km WRF (blue, solid) and RegCM (red, solid) historical ensemble averages, and the 50 km WRF (blue, dotted) and RegCM (red, dotted) historical ensemble averages.

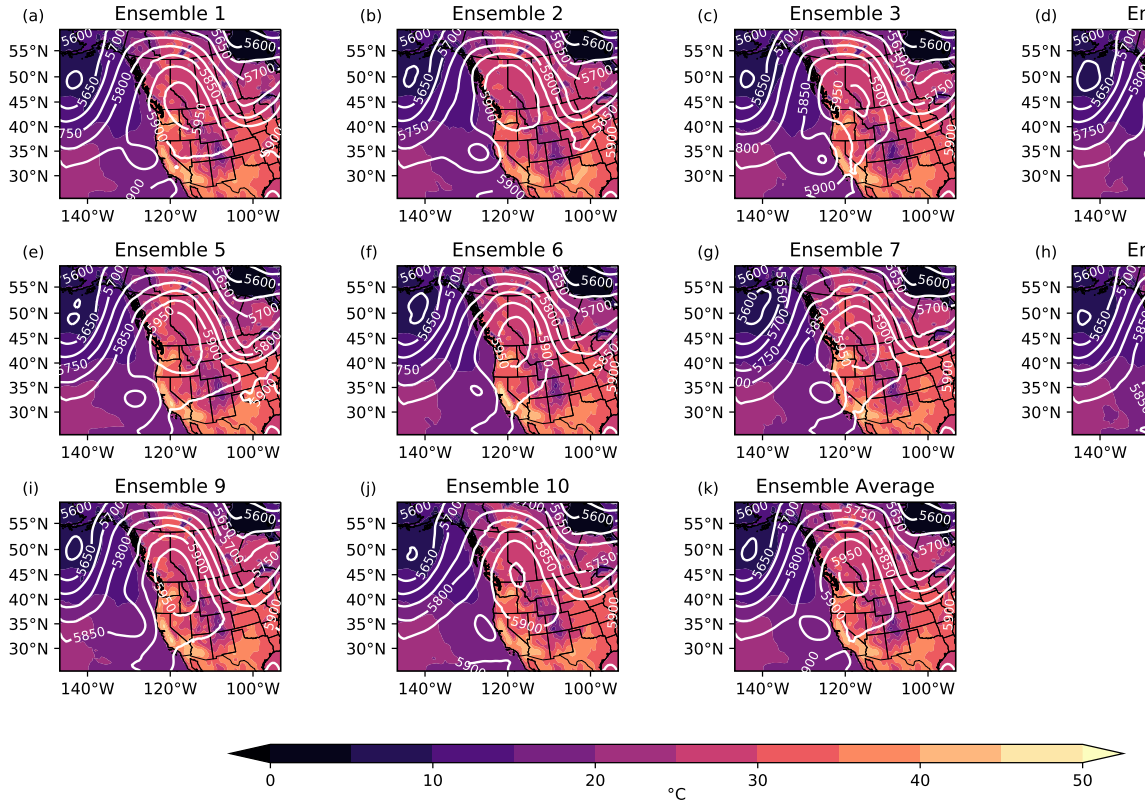

Figure S7. Historical 50 km WRF simulation (a)-(j) individual ensemble members and (k) ensemble-average of the daily maximum 2 m temperature (°C; color contours) and geopotential height at 500 hPa and 0000 UTC (m; white contour lines) on June 28, 2021.

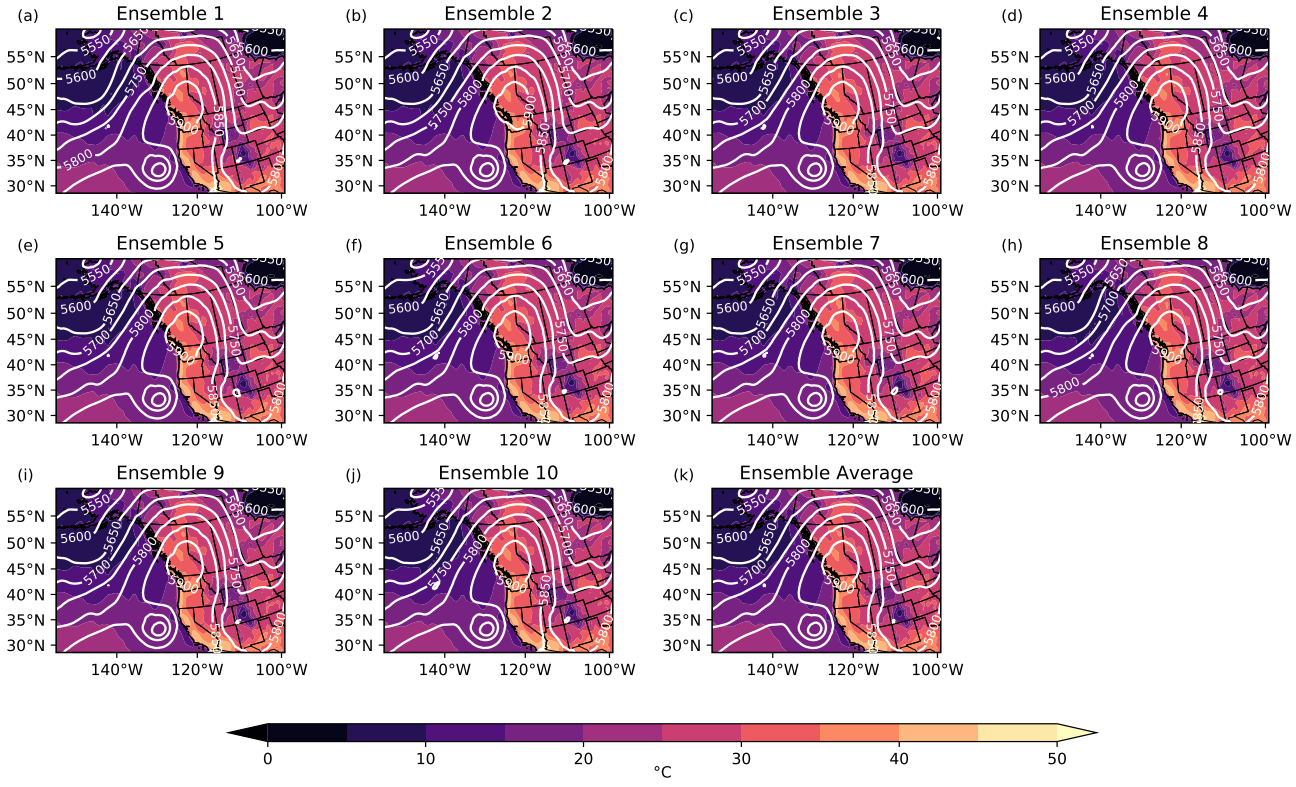

Figure S8. Historical 50 km RegCM simulation (a)-(j) individual ensemble members and (k) ensemble-average of the daily maximum 2 m temperature (°C; color contours) and geopotential height at 500 hPa and 0000 UTC (m; white contour lines) on June 28, 2021.

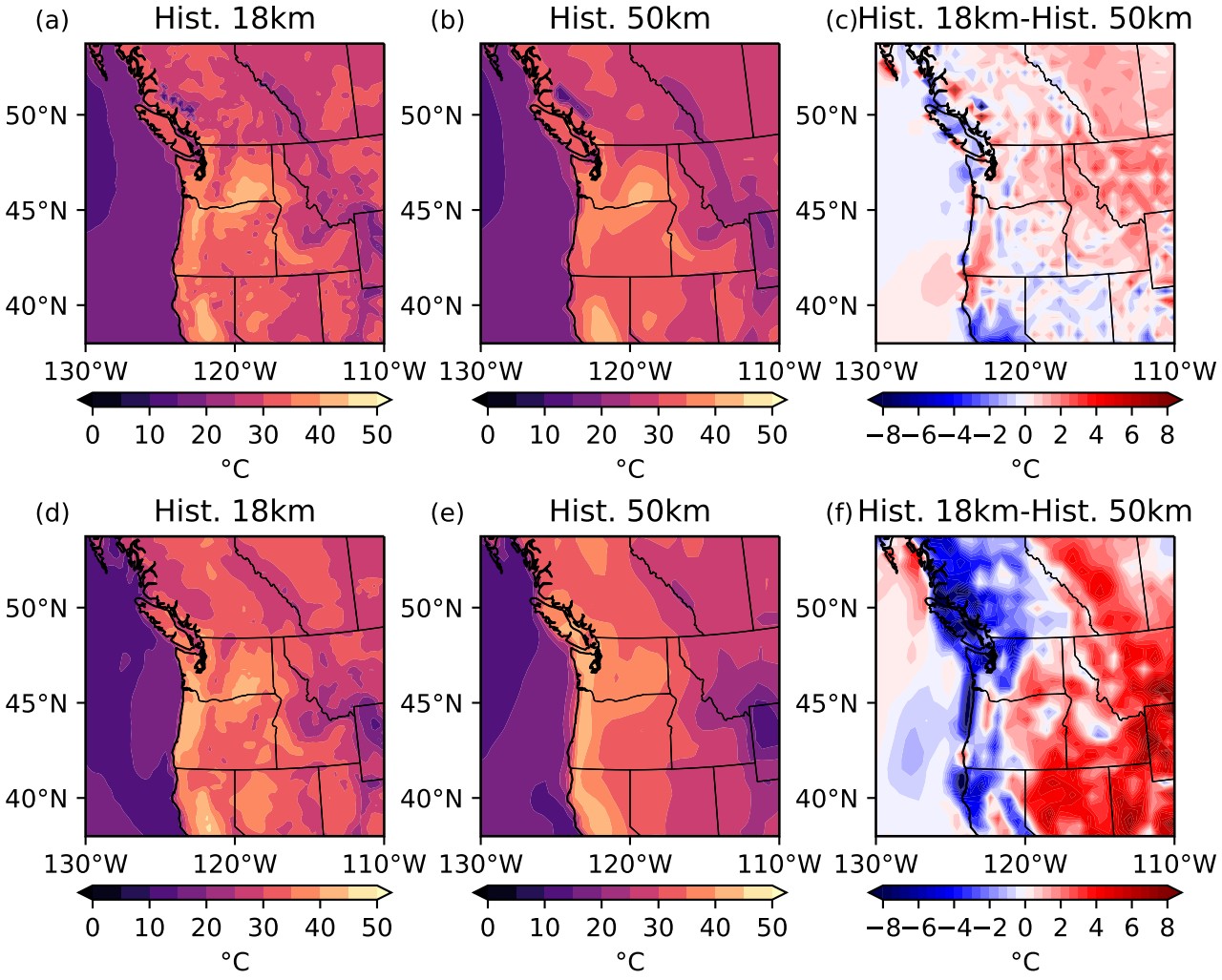

Figure S9. Historical ensemble-averaged daily maximum 2 m temperature (°C; color contours) from WRF at (a) 18 km, (b) 50 km, and (c) 18 km minus 50 km, and RegCM at (d) 18 km, (e) 50 km, and (f) 18 km minus 50 km on June 28, 2021.